

## The composition and structure of the Enceladus plume

C. J. Hansen,<sup>1</sup> D. E. Shemansky,<sup>2</sup> L. W. Esposito,<sup>3</sup> A. I. F. Stewart,<sup>3</sup> B. R. Lewis,<sup>4</sup>  
J. E. Colwell,<sup>5</sup> A. R. Hendrix,<sup>6</sup> R. A. West,<sup>6</sup> J. H. Waite Jr.,<sup>7</sup> B. Teolis,<sup>7</sup> and B. A. Magee<sup>7</sup>

Received 10 March 2011; revised 20 April 2011; accepted 21 April 2011; published 9 June 2011.

[1] The Cassini Ultraviolet Imaging Spectrograph (UVIS) observed an occultation of the Sun by the water vapor plume at the south polar region of Saturn's moon Enceladus. The Extreme Ultraviolet (EUV) spectrum is dominated by the spectral signature of H<sub>2</sub>O gas, with a nominal line-of-sight column density of  $0.90 \pm 0.23 \times 10^{16} \text{ cm}^{-2}$  (upper limit of  $1.0 \times 10^{16} \text{ cm}^{-2}$ ). The upper limit for N<sub>2</sub> is  $5 \times 10^{13} \text{ cm}^{-2}$ , or <0.5% in the plume; the lack of N<sub>2</sub> has significant implications for models of the geochemistry in Enceladus' interior. The inferred rate of water vapor injection into Saturn's magnetosphere is ~200 kg/s. The calculated values of H<sub>2</sub>O flux from three occultations observed by UVIS have a standard deviation of 30 kg/s (15%), providing no evidence for substantial short-term variability. Collimated gas jets are detected in the plume with Mach numbers of 5–8, implying vertical gas velocities that exceed 1000 m/sec. Observations at higher altitudes with the Cassini Ion Neutral Mass Spectrometer indicate correlated structure in the plume. Our results support the subsurface liquid model, with gas escaping and being accelerated through nozzle-like channels to the surface, and are consistent with recent particle composition results from the Cassini Cosmic Dust Analyzer. **Citation:** Hansen, C. J., et al. (2011), The composition and structure of the Enceladus plume, *Geophys. Res. Lett.*, 38, L11202, doi:10.1029/2011GL047415.

### 1. Introduction

[2] On May 18, 2010, the Ultraviolet Imaging Spectrograph (UVIS) on the Cassini spacecraft recorded an occultation of the Sun by the plume of gas and ice particles observed in previous encounters with Saturn's moon Enceladus. This plume was first discovered spewing from fissures across Enceladus' south pole in 2005 [Dougherty et al., 2006; Hansen et al., 2006; Spahn et al., 2006; Waite et al., 2006; Porco et al., 2006]. The energy sources, internal geochemistry and geophysical dynamics that drive this eruption are the subject of ongoing research, constrained by Cassini data.

[3] The Cassini UVIS observations provide measurements of the composition and structure of the gases in the plume. Two previous UVIS observations of stellar occultations employed the far ultraviolet (FUV: 110 to 190 nm) channel and the high speed photometer (HSP) [Esposito et al., 2004]. An occultation of the star  $\gamma$  Orionis was observed in 2005, and from absorption features in the FUV the dominant species was identified as H<sub>2</sub>O [Hansen et al., 2006]. Collimated jets of gas embedded in the plume were detected in the 2007 occultation of the star  $\zeta$  Orionis [Hansen et al., 2008]. The recent occultation of the Sun, reported here, was observed in the solar occultation port of the extreme ultraviolet (EUV) channel, sensitive to wavelengths in the 55 to 110 nm range. The EUV wavelength range includes N<sub>2</sub> absorption features, so the presence or absence of N<sub>2</sub> could be established, a primary objective of the observation. Cassini's Ion Neutral Mass Spectrometer (INMS) observes signal at atomic mass 28 which is ambiguous and attributed to some combination of N<sub>2</sub>, CO, or C<sub>2</sub>H<sub>4</sub> [Waite et al., 2006, 2009]. CO absorption features have not been observed in UVIS data, yielding an upper limit of 3% [Hansen et al., 2008]. This left the species N<sub>2</sub> or C<sub>2</sub>H<sub>4</sub> without independent constraints prior to this new solar occultation data set.

[4] The mixing ratio of N<sub>2</sub> in the plume has significant consequences for models of the geochemistry in the interior, thus it was important for UVIS to provide an independent measurement to resolve the ambiguity in the INMS detection. Is there an internal liquid reservoir? What is its temperature? Is liquid needed at all or could the plume be a result of clathrate decomposition? A strong argument for a liquid source of Enceladus' plume is based on Cassini's Cosmic Dust Analyzer (CDA) observations of entrained grains in the plume containing sodium salts, consistent with an Enceladus ocean in contact with the rocky core [Postberg et al., 2009]. The presence of NH<sub>3</sub> [Waite et al., 2006, 2009] along with N<sub>2</sub> could indicate internal liquid water temperatures of 500–800 K causing dissociation of NH<sub>3</sub>, and/or percolation of liquid through hot rock [Matson et al., 2007]. In a competing model requiring no internal liquids, N<sub>2</sub> has been proposed as a plume propellant via clathrate decomposition [Kieffer et al., 2006].

### 2. Plume Composition

[5] The geometry of the solar occultation was such that the sun's transit behind the plume was tangential to Enceladus' limb, similar to the stellar occultation observed in 2007. Attenuation of EUV sunlight was detected in 95 successive spectra, each integrated over intervals of 1 sec. In the UVIS solar occultation mode the spatial dimension of the solar image is projected onto two windows on the detector, and focused onto 1024 pixels in the spectral dimension, each having a width of 0.606 Å [Esposito et al., 2004]. The

<sup>1</sup>Planetary Science Institute, Tucson, Arizona, USA.

<sup>2</sup>Space Environment Technologies, Altadena, California, USA.

<sup>3</sup>Laboratory for Atmospheric and Space Physics, University of Colorado at Boulder, Boulder, Colorado, USA.

<sup>4</sup>Research School of Physics and Engineering, Australian National University, Canberra, ACT, Australia.

<sup>5</sup>Department of Physics, University of Central Florida, Orlando, Florida, USA.

<sup>6</sup>Jet Propulsion Laboratory, California Institute of Technology, Pasadena, California, USA.

<sup>7</sup>Southwest Research Institute, San Antonio, Texas, USA.

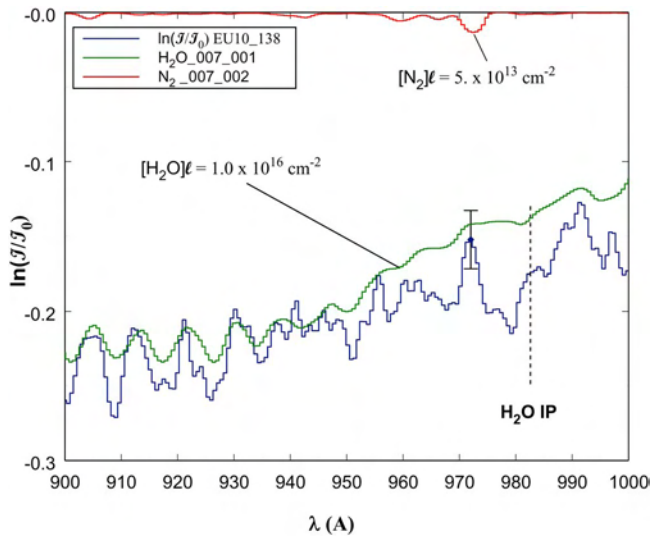


**Figure 1.** The mean extinction spectrum at FWHM of the plume, in the range 900–1000 Å, compared to synthesized forward modeled spectra of H<sub>2</sub>O and N<sub>2</sub>. The mean uses spectra from time records 574 to 618 (elapsed time in seconds, see Figure 3). Coupled-channel calculations by B. R. Lewis and A. N. Heays for N<sub>2</sub> are at a temperature of 150 K and resolution of 10<sup>7</sup> over this range of wavelengths. The H<sub>2</sub>O first ionization potential (IP) and the standard signal count error are shown on the plot. The plotted N<sub>2</sub> extinction spectrum shows the upper limit column density of 5 × 10<sup>13</sup> cm<sup>-2</sup>. The H<sub>2</sub>O extinction spectrum likewise shows the upper limit of 1.0 × 10<sup>16</sup> cm<sup>-2</sup>.

N<sub>2</sub> b(3) – X(0) absorption band at 972 Å is the most sensitive indicator for nitrogen in solar occultations, because the band spectrally aligns with the solar H Lyγ line. The absorption cross-section is temperature sensitive and narrow, requiring coupled-channel [Haverd *et al.*, 2005] model calculations for the low temperature environment and knowledge of solar photon Doppler frequency shift to predict the detailed shape of the absorption transition.

[6] The solar extinction spectrum over the 900–1000 Å wavelength region is shown in Figure 1, compared to a model calculation. The main absorber is recognized to be H<sub>2</sub>O, however fitting the observed spectrum with model calculations is limited by availability of high resolution absorption cross-sections at suitable temperatures. Measurements of the H<sub>2</sub>O photoabsorption cross-section at room temperature by Fillion *et al.* [2003] obtained at a resolution R~640, limited to the energy range above the ionization potential (IP), are used here in the model calculations. Fillion *et al.* [2004] have obtained H<sub>2</sub>O cross-sections at longer wavelengths at high resolution (R~20000), but in the

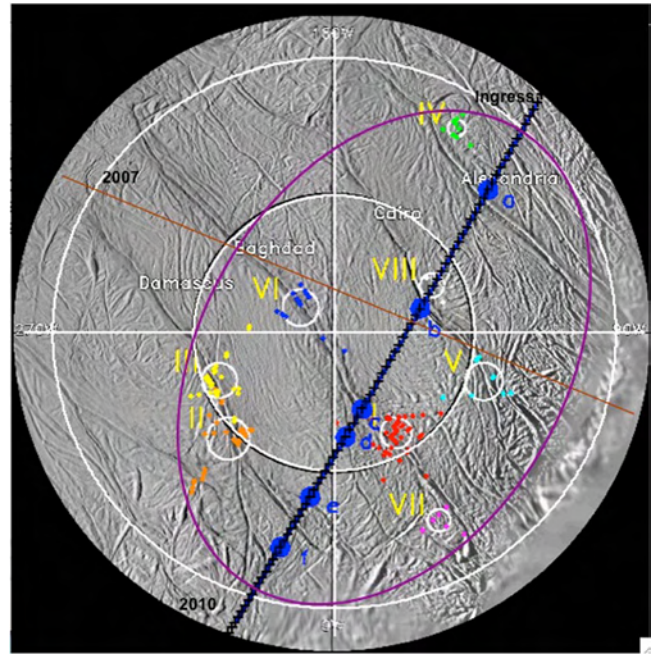


**Figure 2.** On this south polar plot colored dots labeled with Roman numerals show the clusters of dust jet sources mapped by Spitaler and Porco [2007]. The brown line is the ground track of the closest point to Enceladus of a ray from the spacecraft to the star ζ Orionis in the 2007 occultation [Hansen *et al.*, 2008]. The blue line is the ground track of the solar occultation, with large blue dots marking the locations of enhanced gas absorption corresponding to gas jets. The purple ellipse encircles the dust and gas jets. The aspect ratio of the ellipse traversed by the Sun in 2010 compared to the star occultation in 2007 is consistent with the lower column density but equivalent flux.

low-level continuum regions the values are uncertain because of limited dynamic range and variable background. It is evident that in the 900–950 Å region the H<sub>2</sub>O model structure shows good agreement with the data, but the observations show significantly deeper modulation. The upper limit abundance for H<sub>2</sub>O is 1.0 × 10<sup>16</sup> cm<sup>-2</sup>. An H<sub>2</sub>O mixing ratio as low as 0.90 cannot be excluded given the present limit on knowledge of the photoabsorption cross-section properties.

[7] A model calculation for N<sub>2</sub> at a temperature of 150 K is also shown in Figure 1, at the estimated upper limit abundance of 5 × 10<sup>13</sup> cm<sup>-2</sup>. This absorption feature is at the level of the counting statistics standard error shown. Calculations include a Doppler shift in the solar model spectrum (due to heliocentric velocity) of -1.01 × 10<sup>6</sup> cm s<sup>-1</sup>. The UVIS spectrum does not show the N<sub>2</sub> absorption feature at 972 Å, thus establishing an upper limit of <0.5%. With

**Table 1.** The Flux of Water Calculated From the 3 Occultations Observed Using UVIS<sup>a</sup>

Year	$N$ (cm <sup>-2</sup> ), Uncertainty	$y$ (× 10 <sup>5</sup> cm)	$v_{th}$ (cm/s)	Flux: Molecules/s	Flux: Kg/s
2005	$1.6 \times 10^{16} \pm 0.15 \times 10^{16}$	~80	45000	$5.8 \times 10^{27}$	170
2007	$1.5 \times 10^{16} \pm 0.14 \times 10^{16}$	110	45000	$7.4 \times 10^{27}$	220
2010	$0.9 \times 10^{16} \pm 0.23 \times 10^{16}$	150	45000	$6.0 \times 10^{27}$	180

<sup>a</sup>“ $N$ ” is the line-of-sight column density of the water vapor. “ $y$ ” is the width of the plume calculated from the full-width-half-maximum of the occultation event. “ $v_{th}$ ” is the thermal velocity, assumed to be constant in the absence of data to suggest otherwise. Flux =  $N * y * v_{th}$ .

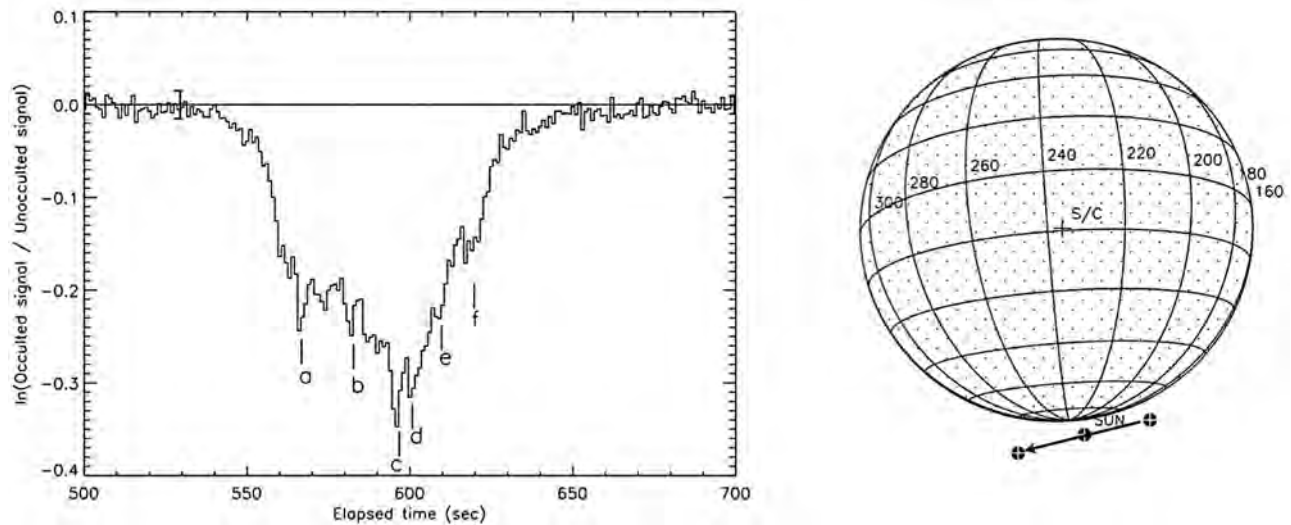


**Figure 3.** The optical depth is shown for the summed wavelength range 850–1000 Å as a function of time. The integration time per record is 1 sec, the width of the steps in the plot. Narrow enhancements in the signal absorption are caused by jets of gas, labeled a–f. The minimum line-of-sight distance from the limb, 20.7 km, occurs between “a” and “b”. The error bar shown on the plot is  $3\sigma$ . The sun followed a path behind the plume tangential to the limb of Enceladus, giving us a roughly horizontal attenuation profile through the plume. With the criteria that the signal is consistently below 98% of the unocculted solar signal the occultation ingress began at 2010 May 18 06:00:48.45 with egress at 06:02:23.45. On the plot elapsed time is relative to the start of the observation at 05:51:44.45. The minimum altitude of the ray (from the sun to UVIS) to Enceladus’ limb was 20.7 km, at 06:01:17.45, at an elapsed time of 574 sec, between features a and b. The projected size of the sun was 1.2 km (smaller than the symbol shown here).

little/no  $N_2$  in the plume the clathrate decomposition model needs to rely entirely on  $CH_4$  as a plume propellant.  $CH_4$  is inherently less volatile than  $N_2$ , and the quantity of  $CH_4$  alone, <1% [Waite *et al.*, 2009], may not be sufficient to produce the detected activity (original calculations were based on a molar ratio of non-condensable gases to water of 10:1) [Kieffer *et al.*, 2006]. The lack of  $N_2$  also means that liquid temperatures  $>500$  K are not required to produce  $N_2$  from dissociation of  $NH_3$ , which reduces internal energy requirements and allows consideration of models with cooler liquids in the interior, such as the “Perrier ocean” proposed by Matson *et al.* [2010].

[8] Quantitative determination of other species in the plume will require a full spectrum absorption cross-section for  $H_2O$  obtained at an appropriately low temperature ( $<200$  K). The mixing ratio of  $CO_2$  for example is loosely constrained to  $<10\%$ .

### 3. Water Vapor Flux

[9] The UVIS spectrum is best fit by a water vapor line-of-sight column density of  $0.90 \pm 0.23 \times 10^{16} \text{ cm}^{-2}$ . Table 1 provides the flux calculation for all three occultations observed using UVIS. The dimensions of the plume are derived from the full-width-half-maximum (FWHM) duration of the occultation multiplied by the Sun’s velocity as seen from the spacecraft across the plane of the sky. From the “tiger stripe” fissures’ surface temperature measured by the Cassini Infrared Spectrometer (CIRS) of at least 170 K [Spencer *et al.*, 2009] the gas thermal velocity is estimated to be at least 450 m/s. (To calculate flux we assume a Maxwell distribution such that the thermal velocity is given by the mean speed of the molecules in the gas =  $((8 \cdot k_B \cdot T) /$

$(\pi \cdot m))^{1/2}$  where  $T$  corresponds to the 170 K surface temperature,  $m$  is the mass of an  $H_2O$  molecule and  $k_B$  is Boltzmann’s constant.)

[10] Given the aspect ratio, illustrated in Figure 2, the flux calculation in 2010 of 180 kg/s is very similar to that of 2005. Recognizing the overall uncertainty, particularly in the thermal velocity, our best estimate of water vapor flux is 200 kg/s. The calculated values of  $H_2O$  flux from all three occultations have a standard deviation of  $\pm 30$  kg/s (15%), inconsistent with any temporal variation as large as a factor of two. This is enough to supply the oxygen detected in the system [Hansen *et al.*, 2006; Melin *et al.*, 2009] via dissociation of water molecules, and suggests that the plume has been stable over the 6 years of the Cassini mission.

### 4. Gas Jets

[11] UVIS data show that gas is ejected along the length of the fissures to make up the broad diffuse plume, while small regions  $<1 \text{ km}^2$  are the sources of the higher density jets of gas. The locations of the gas jets appear to coincide with the dust jets detected by the Cassini Imaging Science Subsystem [Spitale and Porco, 2007; Hansen *et al.*, 2008], illustrated in Figure 2. The solar occultation has better spatial resolution than the 2007 stellar occultation because it was slower and had a much higher signal-to-noise ratio. The optical depth from UVIS spatial window 0, summed over the wavelength range 850–1000 Å, is plotted in Figure 3 as a function of time. The jets are identified as enhanced absorption features that appear in both UVIS spatial windows, ruling out shot noise. Enhanced absorptions in window 0 data are labeled a–f in Figure 3. The density of the jets is  $\sim 3x$  that of the plume, since they show  $\sim 20\%$  increased



**Table 2.** Jet Properties<sup>a</sup>

Enhanced Absorption Feature	Altitude of Ray Relative to Limb	Z <sub>0</sub> : Altitude of Ray Relative to Jet Source	FWHM: Full Width Half Max (km)	Mach Number ~2 * Z <sub>0</sub> /FWHM	Possibly Associated Dust Jet	Excess Signal Attenuation at the Jet (%)
a	21.3	21.6	7	6	Alexandria IV	5
Closest approach	20.7					
b	22	24	9	5	Cairo V and/or VIII	3
c	28.4	29	10	6	Baghdad I	5
d	31.2	36	10	7	Baghdad VII	3
e	39	40	10	8	Damascus III	2
f	47.5	49.7	14	7	Damascus II	2

<sup>a</sup>Six jets are identified in the UVIS data by the attenuation of the solar signal as shown in Figure 3 (in addition to the attenuation of the diffuse plume). Z<sub>0</sub> takes into account the rotation of the source in front of or behind the limb of Enceladus as seen from the spacecraft. The FWHM is determined after removal of the background diffuse plume using a piecewise extrapolation. The excess signal attenuation in column 7 is the difference between the jet attenuation and the background plume attenuation. Correlations to dust jets noted in column 6 may be improved if dust jet locations reported by *Spitale and Porco* [2007] are constrained to lie on the main fissures.

absorption over a spatial scale of 1/15 that of the plume, assuming each feature is due to a single source. Based on the equivalent width of the jets compared to the equivalent width of the plume 3.4% of the observed molecules are in the jets.

[12] The ratio of the intercept altitude in each gas jet (z<sub>0</sub>) to its full-width-half-maximum (FWHM) dimension after subtraction of the diffuse plume shows that the jets are more collimated than estimated from the previous lower resolution data. The Mach number, ~2 × Z<sub>0</sub>/FWHM, ranges from 5 to 8, tabulated in Table 2. To calculate the velocity from the Mach number we use the speed of sound, given by  $(\gamma * k_B * T / m)^{1/2}$ , where  $\gamma$  is 1.33 for a triatomic molecule. For a sound speed of 320 m/s the bulk velocity could exceed 1–2 km/sec (an upper limit because the gas may be cooled in a nozzle). Given the higher velocity of the molecules in the jets, the water vapor flux just in the jets is (5 to 8) \* 3.4% = ~15–25% of the total 200 kg/s flux, thus 30–50 kg/s. The

observed collimation and supersonic velocity of the jets is consistent with the nozzle model developed by *Schmidt et al.* [2008].

[13] The INMS closed ion source [*Waite et al.* 2004] also detected structure in the plume vapor density (Figure 4b) suggestive of gas jets during Cassini's November 2, 2009 Enceladus encounter, which sampled the plume along a trajectory roughly parallel to the 2010 UVIS line of measurement (Figure 4a), and just south of the occultation plane at 91 km closest approach altitude. Water adsorption inside the closed source antechamber inlet introduces measurement time constants of ~15–150 s in the H<sub>2</sub>O signal at 18 daltons, and we therefore use the 44 dalton signal for the more volatile species CO<sub>2</sub> as a proxy for the plume density [*Teolis et al.*, 2010]. Whereas the UVIS remote column density observation includes the broad plume contribution in front of and behind the jets, the INMS detects more jet-to-background amplitude contrast since this instrument senses *in situ*

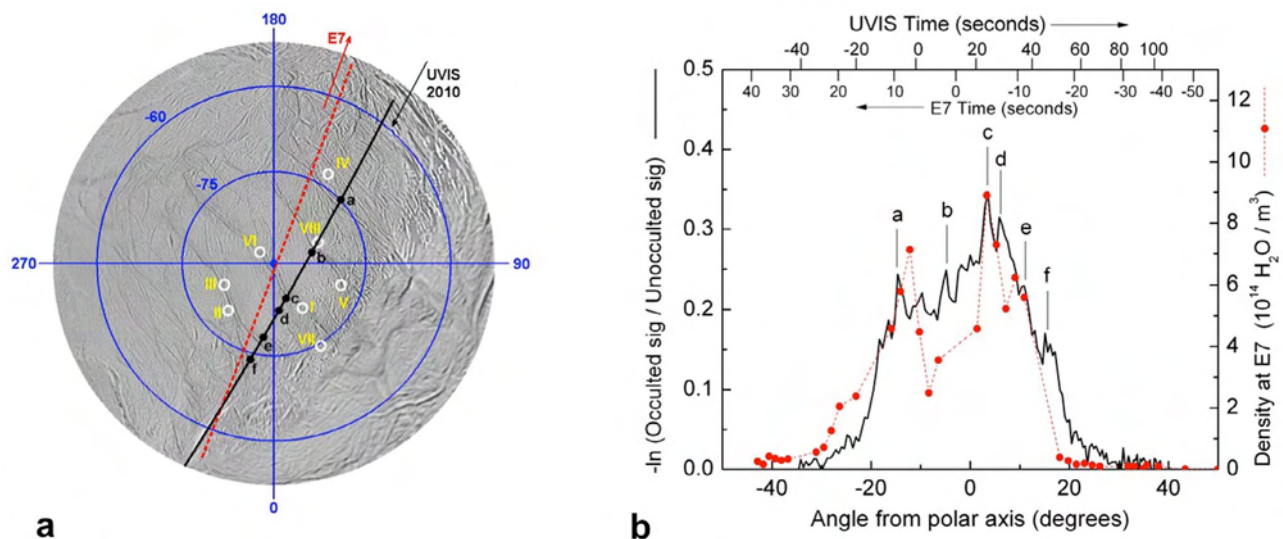


**Figure 4.** (a) The groundtrack of the spacecraft on the E7 flyby, which took place on November 2, 2009, compared to the groundtrack of the ray from the spacecraft to the sun during the solar occultation observed on May 18, 2010. The similarity of the paths allows comparison of the results from INMS, which directly senses the density of molecules in the plume and jets, to the UVIS data. (b) UVIS and INMS measurements are plotted versus angle about the center of Enceladus as viewed from Cassini's position during the 2010 UVIS observation. Time is relative to closest approach for the E7 2009 flyby and relative to minimum ray height for the 2010 solar occultation.

the local density versus position. The detection of fewer features by INMS than UVIS (Figure 4b) is likely due to the relatively poor spatial resolution of the INMS data and insensitivity of the measurement to jets sources distant from Cassini's trajectory. The Alexandria and Baghdad gas jet features detected by UVIS and INMS appear to match when plotted versus angle about the center of Enceladus as viewed from Cassini's 2010 UVIS position (Figure 4b).

[14] The higher density jets may be important for lifting the dust grains to escape velocity and for compositional variations of the grains [Postberg *et al.*, 2011]. The gas partitioning between the diffuse plume and the jets is consistent with compositional differences detected by CDA, with salt-rich grains dominating the diffuse component and salt-poor grains with Enceladus escape velocity predominantly reaching the E ring.

[15] **Acknowledgments.** This work was supported by the Cassini Mission at the Jet Propulsion Laboratory, California Institute of Technology, and the Cassini Data Analysis Program under contracts with the National Aeronautics and Space Administration. The coupled-channel calculations were supported by the Australian Research Council's Discovery Program. The authors thank J.-H. Fillion for providing numerical listings for the H<sub>2</sub>O cross-sections published in 2003 as well as a description of the limits in accuracy and dynamic range; and Tom Spilker for helpful comments.

[16] The Editor thanks Sascha Kempf and an anonymous reviewer for their assistance in evaluating this paper.

## References

- Dougherty, M. K., K. K. Khurana, F. M. Neubauer, C. T. Russell, J. Saur, J. S. Leisner, and M. E. Burton (2006), Identification of a dynamic atmosphere at Enceladus with the Cassini Magnetometer, *Science*, *311*, 1406–1409, doi:10.1126/science.1120985.
- Esposito, L. W., et al. (2004), The Cassini Ultraviolet Imaging Spectrograph investigation, *Space Sci. Rev.*, *115*, 299–361, doi:10.1007/s11214-004-1455-8.
- Fillion, J.-H., F. Dulieu, S. Baouche, J.-L. Lemaire, H. W. Jochims, and S. Leach (2003), Ionization yield and absorption spectra reveal superexcited Rydberg state relaxation processes in H<sub>2</sub>O and D<sub>2</sub>O, *J. Phys. B At. Mol. Opt. Phys.*, *36*, 2767–2776, doi:10.1088/0953-4075/36/13/308.
- Fillion, J.-H., J. Ruiz, X.-F. Yang, M. Castillejo, F. Rostas, and J.-L. Lemaire (2004), High resolution photoabsorption and photofragment fluorescence spectroscopy of water between 10.9 and 12 eV, *J. Chem. Phys.*, *120*, 6531–6541, doi:10.1063/1.1652566.
- Hansen, C. J., L. Esposito, A. I. F. Stewart, J. Colwell, A. Hendrix, W. Pryor, D. Shemansky, and R. West (2006), Enceladus' water vapor plume, *Science*, *311*, 1422–1425, doi:10.1126/science.1121254.
- Hansen, C. J., L. W. Esposito, A. I. F. Stewart, B. Meinke, B. Wallis, J. E. Colwell, A. R. Hendrix, K. Larsen, W. Pryor, and F. Tian (2008), Water vapour jets inside the plume of gas leaving Enceladus, *Nature*, *456*, 477–479, doi:10.1038/nature07542.
- Haverd, V. E., B. R. Lewis, S. T. Gibson, and G. Stark (2005), Rotational effects in the band oscillator strengths and predissociation linewidths for the lowest <sup>1</sup>Π<sub>u</sub> – X <sup>1</sup>Σ<sub>g</sub><sup>+</sup> transitions of N<sub>2</sub>, *J. Chem. Phys.*, *123*, 214304, doi:10.1063/1.2134704.
- Kieffer, S. W., X. Lu, C. M. Bethke, J. R. Spencer, S. Marshak, and A. Navrotsky (2006), A clathrate reservoir hypothesis for Enceladus' south polar plume, *Science*, *314*, 1764–1766, doi:10.1126/science.1133519.
- Matson, D. L., J. C. Castillo, J. Lunine, and T. V. Johnson (2007), Enceladus plume: Compositional evidence for a hot interior, *Icarus*, *187*, 569–573, doi:10.1016/j.icarus.2006.10.016.
- Matson, D. L., T. V. Johnson, J. I. Lunine, and J. C. Castillo-Rogez (2010), Enceladus heat pump model, *Bull. Am. Astron. Soc.*, *42*, 976.
- Melin, H., D. E. Shemansky, and X. Liu (2009), The distribution of atomic hydrogen and oxygen in the magnetosphere of Saturn, *Planet. Space Sci.*, *57*, 1743–1753, doi:10.1016/j.pss.2009.04.014.
- Porco, C. C., et al. (2006), Cassini observes the active south pole of Enceladus, *Science*, *311*, 1393–1401, doi:10.1126/science.1123013.
- Postberg, F., S. Kempf, J. Schmidt, N. Brilliantov, A. Beinsen, B. Abel, U. Buck, and R. Srama (2009), Sodium salts in E-ring ice grains from an ocean below the surface of Enceladus, *Nature*, *459*, 1098–1101, doi:10.1038/nature08046.
- Postberg, F., J. Schmidt, J. Hillier, S. Kempf, and R. Srama (2011), A salt-water reservoir as the source of plumes on Enceladus, *Nature*, in press.
- Schmidt, J., N. Brilliantov, F. Spahn, and S. Kempf (2008), Slow dust in Enceladus' plume from condensation and wall collisions in tiger stripe fractures, *Nature*, *451*, 685–688, doi:10.1038/nature06491.
- Spahn, F., et al. (2006), Cassini dust measurements at Enceladus and implications for the origin of the E Ring, *Science*, *311*, 1416–1418, doi:10.1126/science.1121375.
- Spencer, J. R., A. C. Barr, L. W. Esposito, P. Helfenstein, A. P. Ingersoll, R. Jaumann, C. P. McKay, F. Nimmo, and J. H. Waite (2009), Enceladus: An active cryovolcanic satellite, in *Saturn From Cassini-Huygens*, edited by M. K. Dougherty, L. W. Esposito, and S. M. Krimigis, pp. 683–724, Springer, Dordrecht, Netherlands, doi:10.1007/978-1-4020-9217-6\_21.
- Spitale, J. N., and C. C. Porco (2007), Association of the jets of Enceladus with the warmest regions on its south-polar fractures, *Nature*, *449*, 695–697, doi:10.1038/nature06217.
- Teolis, B. D., M. E. Perry, B. A. Magee, J. H. Westlake, and J. H. Waite (2010), Detection and measurement of ice grains and gas distribution in the Enceladus plume by Cassini's Ion Neutral Mass Spectrometer, *J. Geophys. Res.*, *115*, A09222, doi:10.1029/2009JA015192.
- Waite, J. H., et al. (2004), The Cassini Ion and Neutral Mass Spectrometer (INMS) investigation, *Space Sci. Rev.*, *114*, 113–231, doi:10.1007/s11214-004-1408-2.
- Waite, J. H., et al. (2006), Cassini Ion and Neutral Mass Spectrometer: Enceladus plume composition and structure, *Science*, *311*, 1419–1422, doi:10.1126/science.1121290.
- Waite, J. H., et al. (2009), Liquid water on Enceladus from observations of ammonia and <sup>40</sup>Ar in the plume, *Nature*, *460*, 487–490, doi:10.1038/nature08153.
- J. E. Colwell, Department of Physics, University of Central Florida, 4000 Central Florida Blvd., Orlando, FL 32816, USA.
- L. W. Esposito and A. I. F. Stewart, Laboratory for Atmospheric and Space Physics, University of Colorado at Boulder, 1234 Innovation Dr., Boulder, CO 80303, USA.
- C. J. Hansen, Planetary Science Institute, 1700 E. Fort Lowell, Ste. 106, Tucson, AZ 85719, USA. (cjhansen@psi.edu)
- A. R. Hendrix and R. A. West, Jet Propulsion Laboratory, California Institute of Technology, 4800 Oak Grove Dr., Pasadena, CA 91109, USA.
- B. R. Lewis, Research School of Physics and Engineering, Australian National University, Canberra, ACT 0200, Australia.
- B. A. Magee, B. Teolis, and J. H. Waite Jr., Southwest Research Institute, 6220 Culebra Rd., San Antonio, TX 78238, USA.
- D. E. Shemansky, Space Environment Technologies, 650 Alameda St., Altadena, CA 91001, USA.